Electrical Capacitance Tomography Simulation for Palm Oil Clarifier Applications

Rohani Arpa[1], Nur Tantiyani Ali Othman[1*]

[12*]Department of Chemical and Process Engineering, Faculty of Engineering and Built Environment, Universiti Kebangsaan Malaysia, 43600 UKM Bangi. Selangor, Malaysia

Corresponding author* email: tantiyani@ukm.edu.my
Available online 01 July 2026

ABSTRACT

Electrical capacitance tomography (ECT) is a low-cost and non-invasive technique for imaging multiphase flows. However, its application in palm oil clarification is limited by rectangular tank geometry, internal heating structures, and temperature-dependent permittivity variations. This study develops a multiphysics simulation framework in COMSOL Multiphysics® (v6.2) to evaluate ECT performance in a 20 m × 10 m clarifier equipped with four vertical heating rods and twelve external electrodes. Coupled laminar flow, transient heat transfer, and electrostatics simulations capture buoyancy-driven circulation, where the heating rods generate vigorous central mixing and peripheral low-velocity zones. Mesh independence analysis confirms that the fine mesh accurately resolves thermal and flow gradients with stable convergence. Electric potential simulations at 1, 5, and 10 V indicate that 5 V effectively balances field penetration and stability, while central electrodes yield more symmetric field coverage. These findings offer practical guidelines for electrode placement and excitation strategy, supporting the implementation of ECT as a real-time monitoring tool in palm oil processing.

Keywords: Electrical Capacitance Tomography; Palm Oil Clarifier; COMSOL Multiphysics; Industrial Process Monitoring

1. Introduction

Industrial process monitoring is essential for maintaining efficiency, product quality, and operational safety across complex manufacturing systems [1]–[4]. Electrical capacitance tomography (ECT) has emerged as a promising technique due to its non-intrusive, low-cost, and externally mounted nature, as well as its capability to produce real-time images of dielectric material distributions. Its robustness in harsh operating conditions makes it particularly suited for monitoring non-conductive multiphase flows [4]–[6]. However, applying ECT to clarify the composition of palm oil remains challenging. Clarification tanks are large rectangular vessels equipped with internal heating rods, where geometric complexity, high water content, and thermal gradients distort the electric field distribution. These effects reduce image sensitivity and may lead to negative capacitance readings that hinder reconstruction accuracy [7]–[9]. Temperature-dependent permittivity changes and thermal expansion further complicate measurement stability, requiring monitoring systems that are both geometrically compatible and thermally adaptive [10]–[12].

Most reported ECT studies use simplified cylindrical models for calibration convenience, often assuming binary permittivity contrast, two-dimensional (2D) reconstructions, or static temperature fields, which neglect coupled thermo-fluid interactions present in real clarifiers [3], [6], [13]. This gap is critical in palm oil clarification, where heating induces buoyancy-driven circulation, recirculation zones, and stratification that influence oil–water separation efficiency. Conventional manual sampling methods cannot resolve these transient behaviors at operating temperatures approaching 90°C [6], [14]. Although recent advancements in deep learning-based reconstruction and multimodal sensing (e.g., ECT–electrical resistance tomography fusion) have improved imaging fidelity, industrial implementation remains limited due to cost and integration complexity [10], [12], [15].

To address these limitations, this study develops a multiphysics ECT simulation framework for clarifying palm oil. The model represents a realistic full-scale rectangular clarifier with heating elements and examines how geometry, electrode positioning, and excitation voltage influence electric field distribution and measurement sensitivity. By moving beyond simplified cylindrical assumptions, this work presents a physically representative approach that aligns with industrial mill operations. The findings highlight the potential of ECT as a practical tool for real-time process monitoring in palm oil production, which is significant given that Malaysia and Indonesia together account for more than 85% of global output [16], [17].

2. Methodology

A 2D multiphysics model was developed in COMSOL Multiphysics® (version 6.2) to evaluate the performance of an ECT system in a thermally active palm oil clarifier. The model couples laminar fluid flow, transient heat transfer, and electrostatics to represent realistic operating conditions. A 2D cross-section was selected to reduce computational cost while preserving the dominant thermo-fluid interactions, a common approach in tomography simulation studies where sensor behavior is strongly governed by planar field distribution [18], [19].

2.1 Geometric Domain

The simulation domain (Figure 1) represents a rectangular clarifier equipped with internal heating rods and external electrodes, suitable for pilot-scale systems where direct steam heating is unavailable. Three probe points (P1, P2, and P3) were placed inside the fluid to monitor temporal temperature variations. The electrode dimensions (4 m × 0.25 m) were scaled relative to the clarifier size (20 m × 10 m), with the electrode width selected in accordance with ECT design guidelines recommending widths of approximately 1–5% of the vessel perimeter [5].

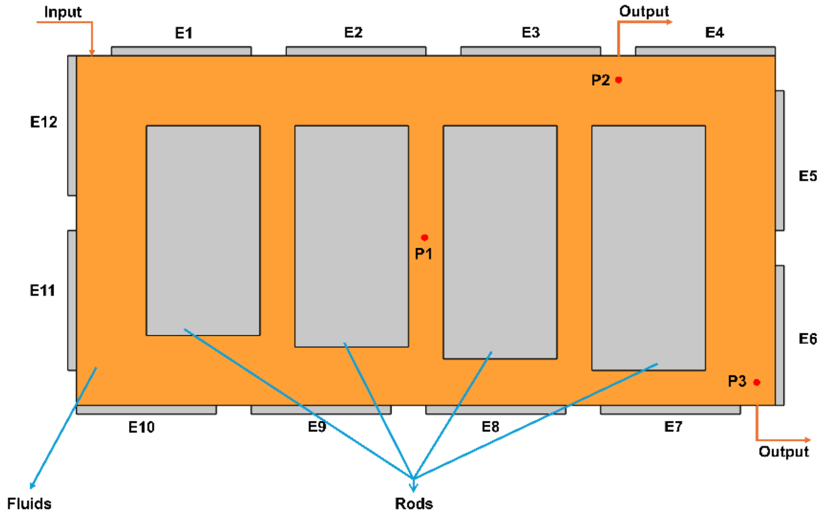

Figure 1. The 2D clarifier domain showing the fluid region, internal heating rods, external electrodes (E1–E12), and probe points P1, P2, and P3 used for temperature monitoring

2.2 Physics Interfaces

Three physics interfaces were used: incompressible laminar flow, conjugate heat transfer, and quasi-static electrostatics. Laminar flow was applied due to the low Reynolds number and buoyancy-driven mixing typical of batch clarifiers [20]. Temperature-dependent properties were assigned to diluted crude oil (DCO) to capture realistic thermo-physical behavior [21]. The heating rods were modeled with a constant heat flux boundary, representing immersion-type heaters commonly used in mills, with simplified dimensions based on typical industrial layouts [22]. ECT excitation was imposed by applying 1, 5, and 10 V to a single electrode while grounding the others, consistent with standard laboratory and industrial excitation ranges [23].

2.3 Meshing and Simulation Studies

A physics-controlled triangular mesh with local refinement around rods and electrodes was used. Mesh independence testing (Figure 2) was conducted on five mesh densities (Coarser to Finer), following mesh quality practices for tomography simulations [24]. Two study modes were conducted:

- **Study A (Time-dependent):** Simulated thermo-fluid evolution for 0–2000s to approach steady-state circulation and temperature distribution.
- **Study B (Stationary):** Solved the ECT forward problem under the three excitation voltages to generate electric potential and permittivity distributions

ECT excitation was implemented using the single-electrode drive method, where one electrode is energized and all others are grounded, as widely used in sensor characterization and reconstruction studies [25]. A summary of model parameters and settings is provided in Table 1.

Table 1. Summary of simulation parameters and model settings

Category	Parameter / Description
Geometry	Rectangular clarifier: 2:1: 20 m × 10 m Four internal vertical heating rods (stainless steel) Twelve external electrodes: 4 m × 0.25 m, evenly spaced Three probe points (P1 at center, P2 and P3 at near outlet)
Materials	Fluid: DCO (Relative permittivity, εr = 3) Solid: Stainless steel (heating rods)
Boundary Conditions	No-slip walls (flow); Adiabatic (heat); Electrically insulated (except active electrodes) Heating rods: Constant heat flux Initial fluid temperature: Uniform
ECT Excitation	One electrode is excited at 1, 5, or 10 V, while the others are grounded.
Physics Interfaces	Laminar Flow (spf); Heat Transfer in Fluids & Solids (ht); Electrostatics (es)
Mesh Configuration	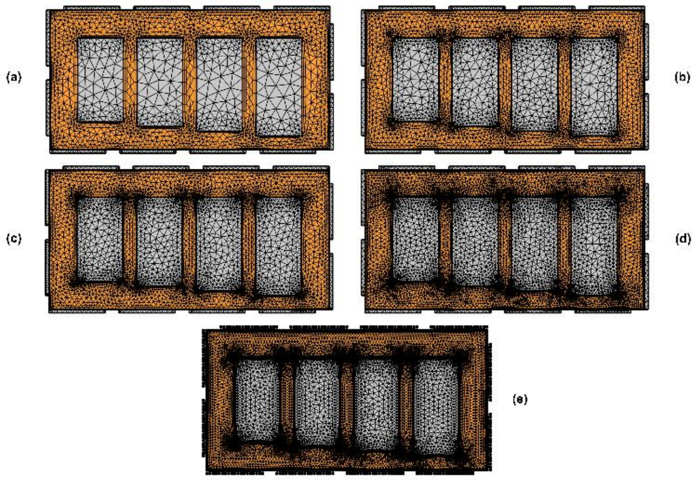 **Figure 2.** Mesh configurations for the clarifier domain: (a) Coarser (3916 elements), (b) Coarse (7031 elements), (c) Normal (9170 elements), (d) Fine (15250 elements), and (e) Finer (23032 elements)
Simulation Studies	Study A (Time-Dependent): 0–2000s; Outputs include temperature, velocity, and probe data Study B (Stationary): Solves the electric potential for three voltage cases

3. Results and Discussion

3.1 Mesh Independence Test

Figure 3 shows the temperature evolution at probe points P1 (10, 5), P2 (15.5, 9.5), and P3 (19.5, 0.5) for five mesh densities. The coarser and coarse grids overpredict heating rates due to insufficient resolution of conduction near the heating rods and buoyancy-driven mixing. In contrast, the normal, fine, and finer meshes produce nearly identical temperature profiles, differing by less than 2–3 K at 2000s, indicating numerical convergence. The temperature at P1 rises fastest due to its proximity to the heating rods, while P2 heats more gradually, reflecting weaker circulation near the upper region. P3 exhibits the lowest temperature rise, confirming reduced thermal influence near the tank boundary. The fine mesh was selected for subsequent simulations to balance accuracy and computational cost based on this convergence behavior.

3.2 Velocity Field Formation

Figure 4 illustrates the development of circulation driven by heating. The velocity increases rapidly during the early warm-up period, rising from approximately 0.0013 m/s to 0.50 m/s, and briefly overshoots to 0.57 m/s at around 400s before stabilizing near 0.51 m/s. This behavior reflects the establishment of buoyancy-driven convection. A central high-velocity plume develops between the heating rods, while lower velocities form near the tank walls and upper region, resulting in a stable single-loop circulation structure. Although vigorous initial mixing may disturb oil–water stratification, the stabilized flow provides sufficient thermal uniformity without excessive shear, essential for effective clarification performance [26].

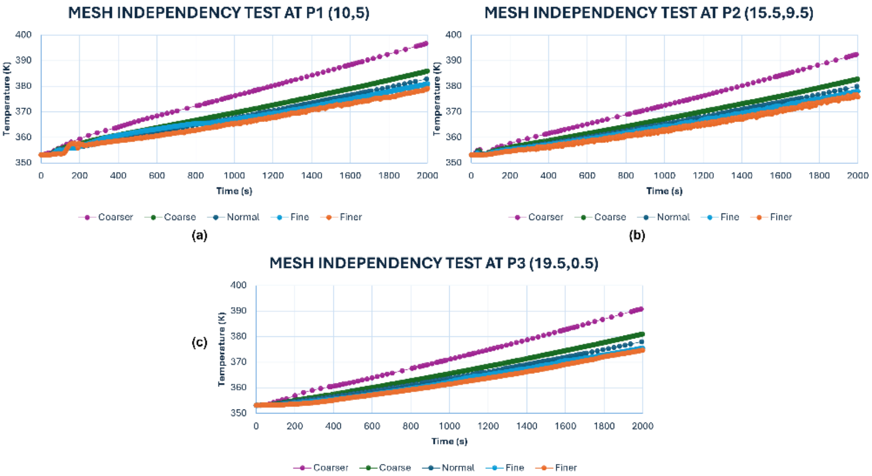

Figure 3. Temperature profiles at probe points: (a) P1 (center), (b) P2 (upper region), and (c) P3 (near boundary) under different mesh configurations during a 2000s simulation

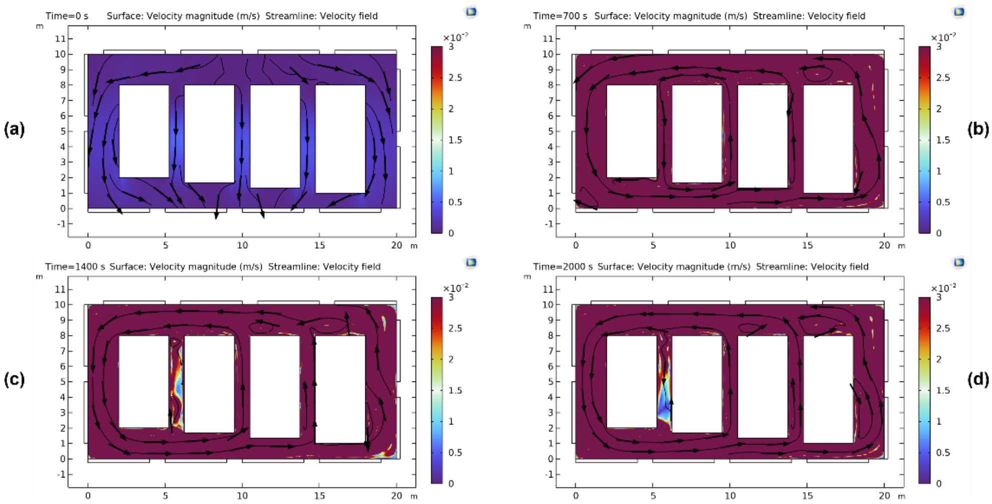

Figure 4. Evolution of velocity streamlines with temperature contours at selected times: (a) 0s, (b) 700s, (c) 1400s, and (d) 2000s, showing the development and stabilization of buoyancy-driven circulation

3.3 Temperature Profile

Figure 5 shows the progression of the temperature field. At 0s, the heating zones surrounding the rods are 400–420 K, while the fluid remains cooler (350–370 K). By the 700s, buoyancy-driven convection distributes heat outward and upward, though pronounced gradients stay near the walls. In the 1400s, the circulation loop strengthened, allowing thermal energy to propagate more uniformly across the tank. By the 2000s, temperature differences were substantially reduced, indicating near-state conditions. The gradual homogenization of the temperature field corresponds to the stabilization observed in the velocity results. It highlights the importance of controlled warm-up time to prevent interfacial disturbance while achieving thermal uniformity conducive to separation.

3.4 Electric Potential

Figures 6(a) and 6(b) show electric potential distributions at 1, 5, and 10 V for Electrodes 1–6 and 7–12, respectively. At 1 V, the electric field is highly localized near the active electrode, yielding limited penetration. At 5 V, the potential contours exhibit uniform spreading with smooth gradients, producing balanced near-wall and interior sensitivity. At 10 V, field penetration increases further, but stronger gradients near boundaries can influence reconstruction stability. Central electrodes (E5–E8) generate the most symmetric field coverage, while corner electrodes (E1–E3, E10–E12) exhibit slight skew due to boundary proximity. Side electrodes (E4, E9) show intermediate penetration shaped by nearby walls and features. These observations indicate that 5 V provides an optimal balance between penetration depth and field uniformity, improving sensitivity to interface motion without amplifying edge effects. Overall, the array behavior is physically consistent and agrees with prior modeling/experiments in clarifiers [23], [29].

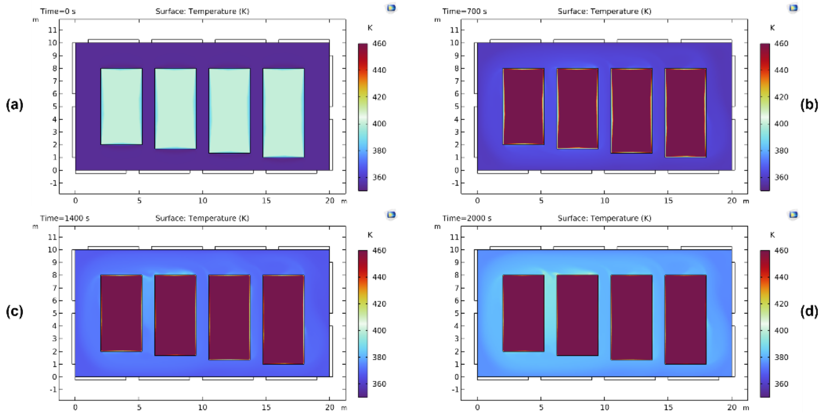

Figure 5. Time-lapse temperature contours in the clarifier at: (a) 0s, (b) 700s, (c) 1400s, and (d) 2000s, highlighting the transition from localized heating to near-uniform thermal distribution

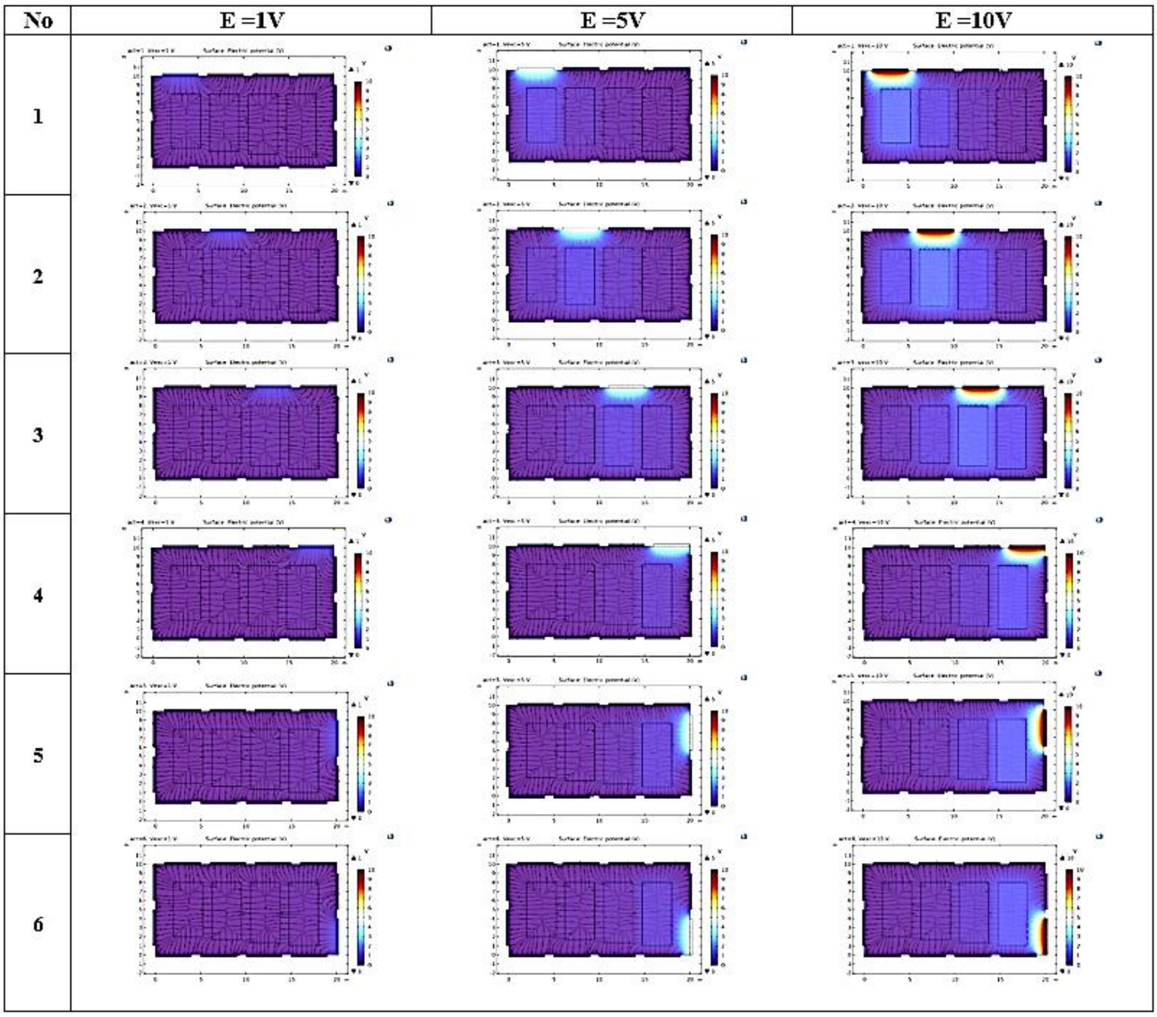

Figure 6 (a). Electric potential distribution for Electrode 1–6 under excitation voltages of 1, 5, and 10 V

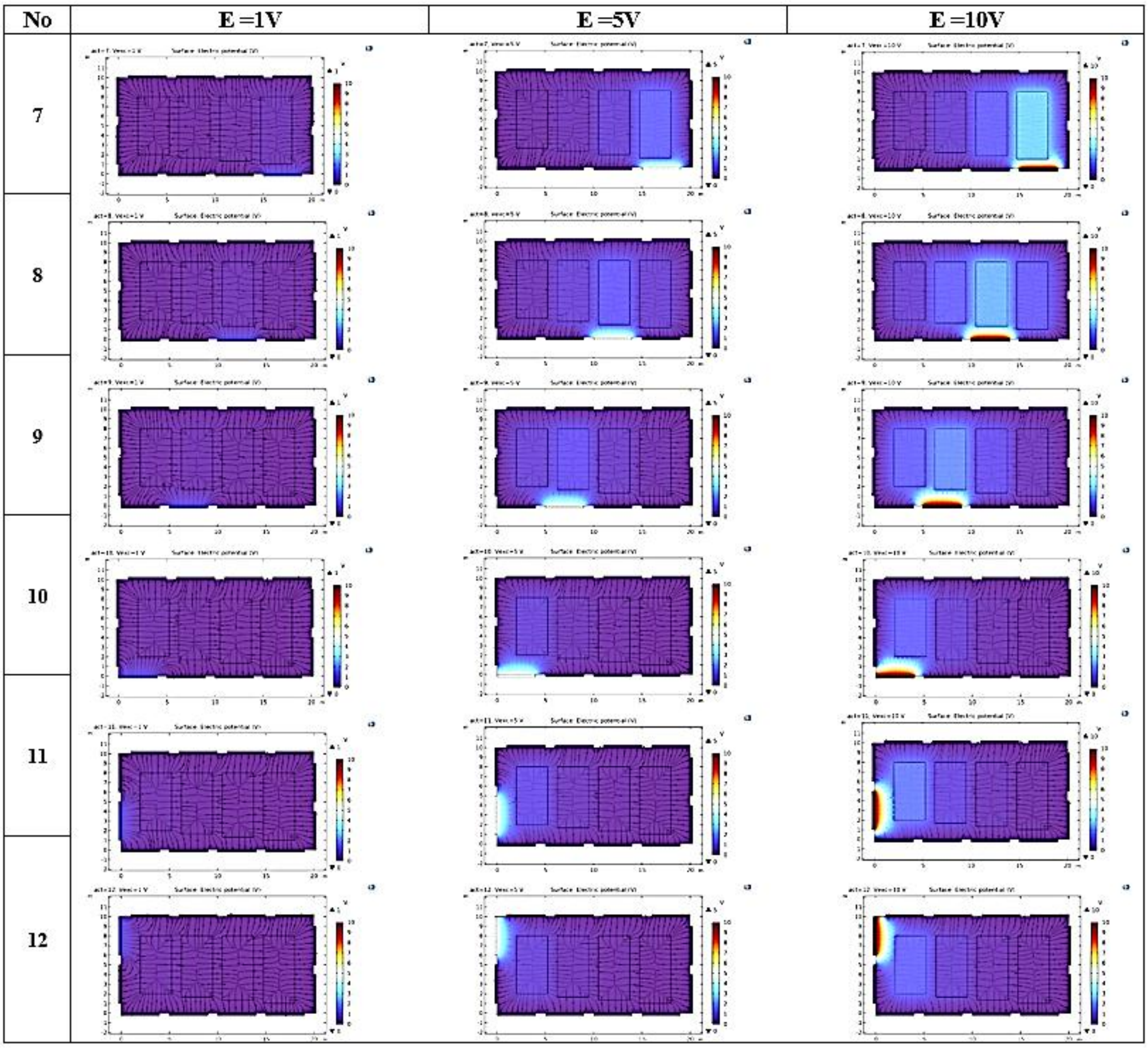

Figure 6 (b). Electric potential distribution for Electrode 7–12 under excitation voltages of 1, 5, and 10 V

3.5 Summary Analysis of Clarification System

Figure 7 summarizes the coupled development of temperature and flow within the clarifier. The crude oil temperature at P2 increases steadily from 353 K to 378 K by the 2000s. Meanwhile, the velocity flow rises rapidly initially, peaking at around 400s. After this initial overshoot, the velocity gradually stabilizes to 0.51 m/s, indicating the establishment of a steady circulation pattern. This behavior reflects buoyancy-driven mixing caused by heating from the rods. The flow becomes stable earlier than the temperature, showing that circulation equilibrates before thermal uniformity is reached. The temperature trend indicates that P2 approaches the critical limit of 371 K (98°C) at approximately 1400–1600s. Therefore, temperature control must prioritize P2 to prevent overheating and preserve oil quality. Operational activities such as separation or sampling should be performed after flow stabilization. Still, before P2 exceeds 371 K. Overall, this figure underscores the importance of coordinated heating and flow management in maintaining stable clarifier performance.

4. Conclusions

This study developed a multiphysics simulation framework to evaluate the feasibility of ECT for real-time monitoring in rectangular palm oil clarifiers. The coupled laminar flow, transient heat transfer, and electrostatics model successfully captured the interactions between internal heating, buoyancy-driven circulation, and permittivity variation in DCO. Mesh independence testing showed that the fine mesh provided accurate thermal and flow predictions with stable numerical convergence. The velocity field results indicated that a stable circulation loop forms with peak central velocities of approximately 0.51–0.57 m/s, while weaker mixing persists near the boundaries. Thermal stabilization occurred at approximately 371–378 K, indicating that the warm-up time must be controlled to prevent disturbing the oil–water interface and maintain clarification efficiency. Electric potential analysis revealed that a 5 V excitation provided the most balanced field penetration and uniformity. At the same time, central electrodes generated more symmetric coverage, supporting a central-prioritized excitation strategy to enhance imaging sensitivity. These findings establish practical guidelines for integrating ECT into industrial clarifiers, particularly in determining electrode placement and heating operation timing. Future work will extend this framework to complete 3D modeling, experimental validation, and real-time reconstruction, thereby advancing the implementation of ECT in sustainable palm oil processing.

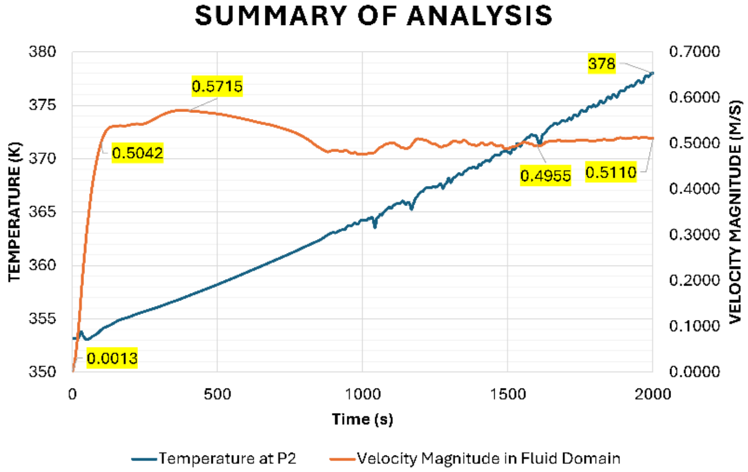

Figure 7. Consolidated thermo-fluid response showing temperature evolution at probe point P2 and stabilized flow velocity, indicating the time required for circulation establishment and temperature uniformity

Acknowledgment

This research is fully supported by the Fundamental Research Grant Scheme (FRGS) grant, FRGS/1/2024/TK05/UKM/02/4. The authors gratefully acknowledge the financial support that enabled the completion and publication of this work.

References

[1] A. Romanowski, B. Szydłowski, P. Gajowniczek, T. Rymarczyk, and D. Sankowski, "Interactive Timeline Approach for Contextual Spatio-Temporal ECT Data Investigation," Sensors, vol. 20, no. 17, p. 4793, 2020, doi: 10.3390/s20174793.

[2] H. Garbaa, L. Jackowska-Strumiłło, K. Grudzień, and A. Romanowski, "Application of Electrical Capacitance Tomography and Artificial Neural Networks to Rapid Estimation of Cylindrical Shape Parameters of Industrial Flow Structure," Archives of Electrical Engineering, vol. 65, no. 4, pp. 657–669, 2016, doi: 10.1515/aee-2016-0046.

[3] B. Przysucha, D. Wójcik, T. Rymarczyk, K. Król, E. Kozłowski, and M. Gąsior, "Analysis of Reconstruction Energy Efficiency in EIT and ECT 3D Tomography Based on Elastic Net," Energies, vol. 16, no. 3, p. 1490, 2023, doi: 10.3390/en16031490.

[4] H. Wang and W. Yang, "Application of Electrical Capacitance Tomography in Circulating Fluidised Beds – A Review," Applied Thermal Engineering, vol. 176, p. 115311, 2020, doi: 10.1016/j.applthermaleng.2020.115311.

[5] W. Yang, "Design of Electrical Capacitance Tomography Sensors," Measurement Science and Technology, vol. 21, no. 4, p. 042001, 2010, doi: 10.1088/0957-0233/21/4/042001.

[6] A. Kowalska, R. Banasiak, A. Romanowski, and D. Sankowski, "3D-Printed Multilayer Sensor Structure for Electrical Capacitance Tomography," Sensors, vol. 19, no. 15, p. 3416, 2019, doi: 10.3390/s19153416.

[7] H. L. M. Ameran, E. J. Mohamad, R. Abdul Rahim, W. N. Abd Rashid, and Z. Mansor, "Design of Crude Palm Oil Monitoring System using Electrical Capacitance Tomography: A Conceptual Framework," International Journal of Advanced Science, Engineering and Information Technology, vol. 7, no. 4, pp. 1374–1380, 2017, doi: 10.18517/ijaseit. 7.4.3145.

[8] M. Weiss, A. Fischerauer, A. Jess, and G. Fischerauer, "Non-Invasive Temperature Monitoring in Fixed-Bed Reactors by Electrical Capacitance Tomography," Measurement Science and Technology, vol. 35, no. 9, p. 095407, 2024, doi: 10.1088/1361-6501/ad5224.

[9] C. Poelma, "Measurement in Opaque Flows: A Review of Measurement Techniques for Dispersed Multiphase Flows," Acta Mechanica, vol. 231, no. 6, pp. 2089–2111, 2020, doi: 10.1007/s00707-020-02683.

[10] R. K. Rasel, S. M. Chowdhury, Q. M. Marashdeh, and F. L. Teixeira, "Review of Selected Advances in Electrical Capacitance Volume Tomography for Multiphase Flow Monitoring," Energies, vol. 15, no. 14, p. 5285, 2022, doi: 10.3390/en15145285.

[11] F. Wang, Q. Marashdeh, L.-S. Fan, and W. Warsito, "Electrical Capacitance Volume Tomography: Design and Applications," Sensors, vol. 10, no. 3, pp. 1890–1917, 2010, doi: 10.3390/s100301890.
[12] M. Neumayer, A. Schuster, M. Weber, K. Rehak, and M. Kogler, "ECT in a Large Scale Industrial Pneumatic Conveying System," Measurement Science and Technology, vol. 35, no. 9, p. 096002, 2024, doi: 10.1088/1361-6501/ad42c0.
[13] R. Banasiak, M. Bujnowicz, and A. Fabijańska, "Study on Quality Assessment Methods for Enhanced Resolution Graph-Based Reconstructed Images in 3D Capacitance Tomography," Applied Sciences, vol. 14, no. 22, p. 10222, 2024, doi: 10.3390/app142210222.
[14] E. J. Mohamad, R. A. Rahim, P. L. Leow, M. H. F. Rahiman, O. M. F. Marwah, and N. M. N. Ayob, "Visualization of Recovered Palm Oil Using Portable ECT Imager in Extraction Palm Oil Process," Flow Measurement and Instrumentation, vol. 31, pp. 61–68, 2013, doi: 10.1016/j.flowmeasinst.2012.10.004.
[15] J. Porzuczek, "Applications of Electrical Capacitance Tomography for Research on Phenomena Occurring in the Fluidised Bed Reactors," Chemical and Process Engineering, vol. 35, no. 4, pp. 397–408, 2014, doi: 10.2478/cpe-2014-0030.
[16] H. Silvamany, R. Raja, R. Subramaniam, M. Mohd Noor, and S. M. Sidik, "Engineering Solutions for the Palm Mill of the Future: Increasing Extraction Rate and Sustainability Through Biotechnology," IOP Conference Series: Materials Science and Engineering, vol. 1195, no. 1, p. 012061, 2021, doi: 10.1088/1757-899X/1195/1/012061.
[17] H. L. M. Ameran, E. J. Mohamad, S. Z. M. Muji, R. A. Rahim, J. Abdullah, and W. N. A. Rashid, "Multiphase Flow Velocity Measurement of Chemical Processes Using Electrical Tomography: A Review," in Proceedings of the 2016 IEEE International Conference on Automatic Control and Intelligent Systems (I2CACIS), Selangor, Malaysia, pp. 162–167, 2016, doi: 10.1109/i2cacis.2016.7885308.
[18] M. A. Zimam, E. J. Mohamad, R. Abdul Rahim, and L. Pei Linga, "Sensor Modelling for an Electrical Capacitance Tomography System Using COMSOL Multiphysics," Jurnal Teknologi, vol. 55, no. 2, pp. 33–47, 2012.
[19] COMSOL, "Creating 2D Models from 3D Geometries in COMSOL Multiphysics®." [Online]. Available: https://www.comsol.com/video/creating-2d-models-from-3d-geometries-in-comsol-multiphysics.
[20] COMSOL, "Introduction to Conjugate Heat Transfer Modeling in COMSOL Multiphysics®." [Online]. Available: https://www.comsol.com/support/learning-center/article/introduction-to-conjugate-heat-transfer-modeling-in-comsol-multiphysics-90531/242.
[21] COMSOL, Heat Transfer Module User's Guide. COMSOL, 2018. [Online]. Available: https://doc.comsol.com/5.4/doc/com.comsol.help.heat/HeatTransferModuleUsersGuide.pdf.
[22] Kalapa Sawit – Lestari, "Clarification (Palm Oil Mill)." [Online]. Available: https://sawitlestari.blogspot.com/2015/11/clarification-palm-oil-mill.html.
[23] N. A. Abd. Rahman, R. A. Rahim, M. H. F. Rahiman, and F. H. Fauzi, "A Review on Electrical Capacitance Tomography Sensor Development," Jurnal Teknologi, vol. 73, no. 3, pp. 35–41, 2015, doi: 10.11113/jt.v73.4244.
[24] COMSOL, Optimization Module User's Guide. COMSOL, 2023. [Online]. Available: https://doc.comsol.com/6.2/doc/com.comsol.help.opt/OptimizationModuleUsersGuide.pdf.
[25] K. Manikandan and S. Sathiyamoorthy, "Modeling and Implementation of AC Electrical Capacitance Tomography," Circuits and Systems, vol. 7, no. 11, pp. 3818–3830, 2016, doi: 10.4236/cs.2016.711319.
[26] A. H. Mohammad Fauzi, M. N. A. A. Saifuddin, F. H. Kasim, and Z. Y. Zakaria, "Simulation of Crude Palm Oil Dilution and Clarification in a Palm Oil Mill Using Computational Fluid Dynamics: Grid Dependency and Parametric Studies," IOP Conference Series: Earth and Environmental Science, vol. 765, no. 1, p. 012106, 2021, doi: 10.1088/1755-1315/765/1/012106.
[27] Y. M. Thang, M. R. Mohd Kasim, H. M. Musa, and Z. Zakaria, "Roles and Principles of Sterilisation Process in Palm Oil Mills," Pertanika Journal of Science and Technology, vol. 29, no. 4, pp. 1749–1762, 2021, doi: 10.47836/pjst. 29.4.26.
[28] S. Pakdeechot, S. Hanifarianty, and M. Wae-hayee, "The Effects of Sterilization Time of FFB on Fruit-Bunch Separation and Crude Palm Oil Quality Using Direct Steaming," Journal of Advanced Research in Applied Mechanics, vol. 72, no. 1, pp. 1–9, 2020, doi: 10.37934/aram. 72.1.19.
[29] E. J. Mohamad, R. A. Rahim, M. H. F. Rahiman, H. L. M. Ameran, Y. A. Wahab, and O. M. F. Marwah, "Analysis of Crude Palm Oil Composition in a Chemical Process Conveyor Using Electrical Capacitance Tomography," Flow Measurement and Instrumentation, vol. 50, pp. 57–64, 2016, doi: 10.1016/j.flowmeasinst.2016.06.011.